RSC Advances

ROYAL SOCIETY OF CHEMISTRY

www.rsc.org/advances

Cite this: DOI: 10.1039/c0xx00000x

www.rsc.org/xxxxxx

ARTICLE TYPE

Hybrid Lanthanide Complexes Based on a Novel β–Diketone Functionalized Polyhedral Oligomeric Silsesquioxane (POSS) and Their Nanocomposites with PMMA *via* in Situ Polymerization

Liguo Li, Shengyu Feng, and Hongzhi Liu*

Received (in XXX, XXX) Xth XXXXXXXXX 20XX, Accepted Xth XXXXXXXXX 20XX
DOI: 10.1039/b000000x

A novel β–diketone–functionalized POSS dendrimer was initially prepared from octamercaptopropyl–substituted polyhedral oligomeric silsesquioxane (POSS) and diethyl allylmalonate by photochemical thiol–ene reaction. The POSS dendrimer was used as a ligand to coordinate with lanthanide ions (Eu^{3+} and Tb^{3+}) to form hybrid luminescent complexes. The resulting hybrid lanthanide complexes were incorporated into PMMA matrix *via* in situ polymeration. Morphology study suggested that these hybrid complexes assembled into spherical particles with a diameter of approximately 100 nm and could be well dispersed in PMMA matrix. The resultant hybrid luminescent PMMA based on POSS exhibited highly saturated color and good thermal stability.

Introduction

Development of luminescent lanthanide ion (Ln^{3+}) complexes based on energy transfer mechanisms is extensive and has drawn considerable attention because of their academic significance and potential applications,[1–4] such as in medical diagnostics,[5] biological imaging[6] and optical amplifiers.[7] To further enhance amplified luminescence intensity, design and synthesis of some novel ligands are necessary to excite Ln^{3+} ions *via* energy transfer from ligands to Ln^{3+} ions.

Dendrimers are hyperbranched 3D macromolecules with a pseudo network structure that potentially trap guest molecules.[8,9] In particular, dendrimer–bearing binding sites for metal ions are eliciting much attention.[10] The dendrimer structure has been selected as a basis for the formation of polymetallic lanthanide complexes.[11,12] The use of dendrimers is an efficient and versatile approach to increase the luminescence of the compound. This approach is performed by incorporating larger numbers of chromophoric groups and several lanthanide cations into one discrete molecule. The classical approach in lanthanide chemistry involves using one Ln^{3+} to bind several ligands, whereas this system uses one branched ligand to bind several lanthanides and chromophores. This approach is a simple strategy to maximize the luminescence of lanthanide complexes.[13] The high absorption extinction coefficients of these modified dendrimer molecules allow them to absorb a large amount of energy that can be used to sensitize the coordinated lanthanide ions.[14] Lanthanide ions can be incorporated in each region of the globular dendritic structure, which is expected to shield the lanthanide cations from deactivation through solvent vibrations.[15] The sensitizers of this strategy are not required to directly bind to metal ion, allowing for a broader choice of lanthanide sensitizers.

Polyhedral oligomeric silsesquioxane (POSS) are of considerable interest owing to its unique cage–like molecular structure containing an inorganic silica core surrounded by organic groups.[16] They provide an excellent platform for the synthesis of new inorganic–organic hybrid materials with enhanced thermal and mechanical properties.[17–19] Some interest hybrid electronic and photonic materials derived from POSS were also prepared.[20–23] Recently, mercaptopropyl substituted POSS were used as ligands for Au[24] or tailoring CdSe quantum dots (QDs),[25,26] which were used as novel fluorescent sensors. The well–defined POSS, almost cubic silica–like core surrounded by eight organic groups (R) makes them topologically ideal for the preparation of dendritic molecules, where a large number of external branching sites on the core lead to a high concentration of dendrimer branch ends after relatively few generations.[27] The preparation of some dendritic ligands using POSS as cores and their complexes with lanthanide ions are rarely reported. In this study, octamercaptopropyl substituted POSS was chosen as a starting material to react with diethyl allylmalonate to produce a β–diketone functionalized POSS dendrimer, which could complex with lanthanide ions.

β–diketone rare earth complexes have been investigated for a long time.[28] These highly functional complexes exhibit outstanding photophysical, electric, and magnetic properties. In particular, the optical property has a wide range of applications, from phosphors to photo/electro–luminescent devices, optical amplifiers and generation and amplification of light in lasers.[29–31] However, these existing β–diketone rare earth complexes are restricted from practical applications because of their poor thermal stability and low mechanical strength. An appropriate approach is to introduce a stable rigid ligand into the complexes.[32,33] β–diketone–functionalized POSS dendrimer is a promising ligand to overcome these limitations through

incorporation of POSS with good thermal and mechanical stability.

The incorporation of nanoparticles (NPs) containing lanthanide ions into polymer matrices to obtain new transparent hybrid nanocomposites is a sector of recent interest.[34–36] In fact, hybrid polymer nanocomposites are appealing because of their improved properties and unique combination of characteristics.[37,38] In situ polymerization of NPs into polymer matrices to obtain bulk polymer–NP composites often results in the loss of transparency in the final product due to the occurrence of phase separation.[34,39] Gulino *et al.* once proposed a bottom–up strategy to prepare a monolayer of the tris–(dibenzoylmethane) mono(5–amino–1,10–phenanthroline)–europium(III) complex covalent–assembled on top of a film composed of polystyrene chains that, in turn, were covalently grown perpendicular to the Si(100) surface by an atom transfer radical–polymerization reaction. [40, 41]

This paper reports the preparation of new transparent nanocomposites consisting of hybrid luminescent complexes derived from β–diketone–functionalized POSS dendrimer embedded in poly(methyl methacrylate) (PMMA) matrixes *via* in situ polymerization. PMMA was chosen because of its transparency and ductility characteristics. The present approach is divided into four steps: (1) the synthesis of POSS dendrimer; (2) the synthesis of hybrid complexes with Eu^{3+} or Tb^{3+}; (3) the incorporation of hybrid complexes into methyl methacrylate (MMA); (4) in situ polymerization. The hybrid complexes based on POSS and their nanocomposites with PMMA were investigated by Fourier transform infrared spectroscopy (FT–IR), X–ray photoelectron spectroscopy (XPS), powder X–ray diffraction (PXRD), polarized optical microscopy (POM), small–angle X–ray scattering (SAXS), transmission electron microscopy (TEM), dynamic light scattering (DLS), ultraviolet (UV) absorption, fluorescence, and thermal gravimetric analysis (TGA).

Experimental Section

Materials

Starting materials (diethyl malonate and allyl bromide) and solvents were purchased from China National Medicines Group and used without further purification. 2,2–Dimethoxy–2–phenylacetophenone (DMPA) was purchased from Aldrich and used as received. Methyl methacrylate was distilled before use. Europium and terbium nitrates were obtained from their corresponding oxides in strong nitric acid. Octamercaptopropyl–substituted silsesquioxanes (POSS_SH) were prepared according to the literature.[42] Similarly, diethyl allylmalonate was synthesized according to the literature.[43]

Characterization

The reaction was irradiated by high–intensity UV (365 nm) on a Spectroline Model SB–100P/FA lamp. FT–IR spectra were measured within a 4000 cm^{-1} to 400 cm^{-1} region on a Bruker TENSOR–27 infrared spectrophotometer (KBr pellet). ^1H NMR, ^{13}C NMR, and ^{29}Si NMR spectra were recorded in $CDCl_3$ on a Bruker Avance–400 spectrometer without internal reference. A MALDI–FTMS experiment was conducted using a 7.0T SolariX FTMS system equipped with a MALDI source (Bruker Daltonics). The intensity of MALDI–laser irradiation was 15% with frequency at 1000Hz in positive–ion reflection mode using dithranol as the matrix, and $AgNO_3$ as the ion source. UV absorption spectra of these samples (in THF solution) were recorded using a Beijing TU–1901 double beam UV–vis spectrophotometer. TGA was performed on a Mettler Toledo TGA/DSC1 with heating rate of 10 °C/min from 25 °C to 800 °C under N_2 (100 mL/min) at ambient pressure. The luminescence (excitation and emission) spectra and the fluorescence quantum yields (FQY) were measured on Hitachi F-4500 fluorescence spectrophotometer equipped with the Quantum Yield measuring accessory and Report Generator program. All the information provided applies to this system. For solid samples, emission quantum yield was calculated from corrected emission spectra registered by Hitachi F-4500 fluorescence spectrophotometer equipped with an intergrating sphere (60 mm), a Al_2O_3 white tiles, a 150 W Xe lamp (λ excitation tunable by a monochromator supplied with the instrument) as light source, and a R928 photomultiplayer.PXRD patterns were recorded on a RiauD/Max 2200PC diffractometer equipped with Cu Co radiation at 40 kV/20 mA (λ = 1.542 Å). The scanning rate was 10°/min from 2θ = 6° to 80°. SAXS experiments were performed on Anton Par Saxes mc^2 with Cu Kα radiation at 40 kV/50 mA (λ = 1.542 Å) at room temperature. XPS measurements were carried out using a Thermo Scientific Esca Lab 250 Xi XPS spectrometer with a monochromatic AlKα source (1486.6 eV). The binding energy of C_{1s} at 284.6 eV was used as the standard. DLS measurements were performed on a multi–angle laser photometer equipped with a linearly polarized gallium arsenide (GaAs) laser (k = 658 nm; Wyatt Technology Co. DAWN HELEOS). The measurements were conducted at a scattering angle of 99°. TEM graphs were examined under a microscope (JEM–1011 TEM; 100 kV) at room temperature. The ultrathin membrane sample for TEM of PMS was prepared by an ultramicrotome of model Ultracut-R made by Leica, using a diamond.

.

Synthesis of POSS_dendrimer

POSS_dendrimer was prepared by photochemical thiol–ene reaction.[44] POSS_SH (2.0 g; 2.0 mmol), diethyl allylmalonate (3.4 g; 16.8 mmol), and DMPA (0.1 g; 2 wt%) were charged to a transparent bottle with 10 mL of THF. After the chemicals were dissolved in THF, the mixtures were irradiated by UV lamp for 30 min.[45] Then, the THF was removed by vacuum rotary evaporation. The resulting oil was washed thrice by petroleum ether and dried overnight to obtain a yellow viscous oil in high yield (98.7%). ^1H NMR ($CDCl_3$, 400 MHz): δ 0.76–0.78 (t, 16H, –SiC$\underline{H}_2$), 1.24–1.31 (t, 48H, –COOCH_2C$\underline{H}_3$), 1.59–1.65 (m, 32H, –SCH_2C$\underline{H}_2$C$\underline{H}_2$CH), 1.98–2.07 (m, 16H, –Si–CH_2C$\underline{H}_2$), 2.52–2.57 (m, 32H, –C$\underline{H}_2$SC$\underline{H}_2$–), 3.33–3.38 (t, 8H, –C$\underline{H}$COO–), 4.16–4.25 (m, 32H, –COOC$\underline{H}_2$CH$_3$); ^{13}C NMR ($CDCl_3$, 100 MHz): δ 14.04, 14.61, 22.92, 27.16, 27.79, 31.28, 38.11, 51.52, 61.26, 169.14; ^{29}Si NMR ($CDCl_3$, 80 MHz): δ −67.26. Anal. calcd for $C_{104}H_{184}O_{44}S_8Si_8$: C 47.68, H 7.08, S 9.79; found: C 47.89, H 7.07, S 9.55. MALDI–FTMS Calcd for $C_{104}H_{184}O_{44}S_8Si_8$ + dithranol + H^+: m/z 2846.98 [M + dithranol + H]$^+$. Found: m/z 2847.77.

Preparation of hybrid luminescent complexes based on POSS_dendrimer

A series of complexes were prepared following the same procedure (Table 1). POSS_dendrimer (0.2 g; 0.08 mmol) and europium nitrate (0.04 g 0.08 mmol) were charged to a bottle with 3 mL of THF. The mixtures were sufficiently stirred for 24 h at room temperature, then THF was removed by rotatory evaporation. The resulting mixtures were dissolved in 10 mL $HCCl_3$ and washed by 10 mL distilled water for three times. Subsequently, the organic layer was separated and the chloroform were removed under vacuum. Finally, a yellow transparent solid was obtained (denoted as POSS_Eu_1).

Table 1 Various ratios of POSS_Ln (Ln = Eu, Tb) complexes

Sample name	Molar ratios	POSS/g	$Ln(NO_3)_3 \cdot 6H_2O$/g
POSS_Ln_1	1:1	0.20	0.04
POSS_Ln_2	1:2	0.20	0.07
POSS_Ln_3	1:3	0.20	0.10
POSS_Ln_4	1:4	0.20	0.14

Preparation of hybrid PMMA nanocomposites from hybrid complexes (denoted as PMS_Ln)

POSS_Ln_3 was embeded into PMMA matrix to prepare hybrid nanocomposites with different doping concentrations (5, 10 wt %) *via* in situ polymerization. For example, 0.05 g POSS_Eu_3 was dissolved in 0.5 mL THF, and then MMA (1.0 g) and 0.02 g BPO were added to the solution. The mixture was sonicated for 10 min to disperse hybrid complex. After that, THF was removed under vacuum at room temperature. The mixture was heated at 60 °C for 2 h, 70 °C for 1 h, and 95 °C for 36 h to to ensure the polymerization was complete. The obtained hybrid nanocomposite was a transparent solid. Pure PMMA and hybrid PMMA materials with 10 wt% POSS complexes were also prepared, respectively, following the same process. These hybrid PMMA solids also exhibited nice photoluminescence when excited at 365 nm by a UV light.

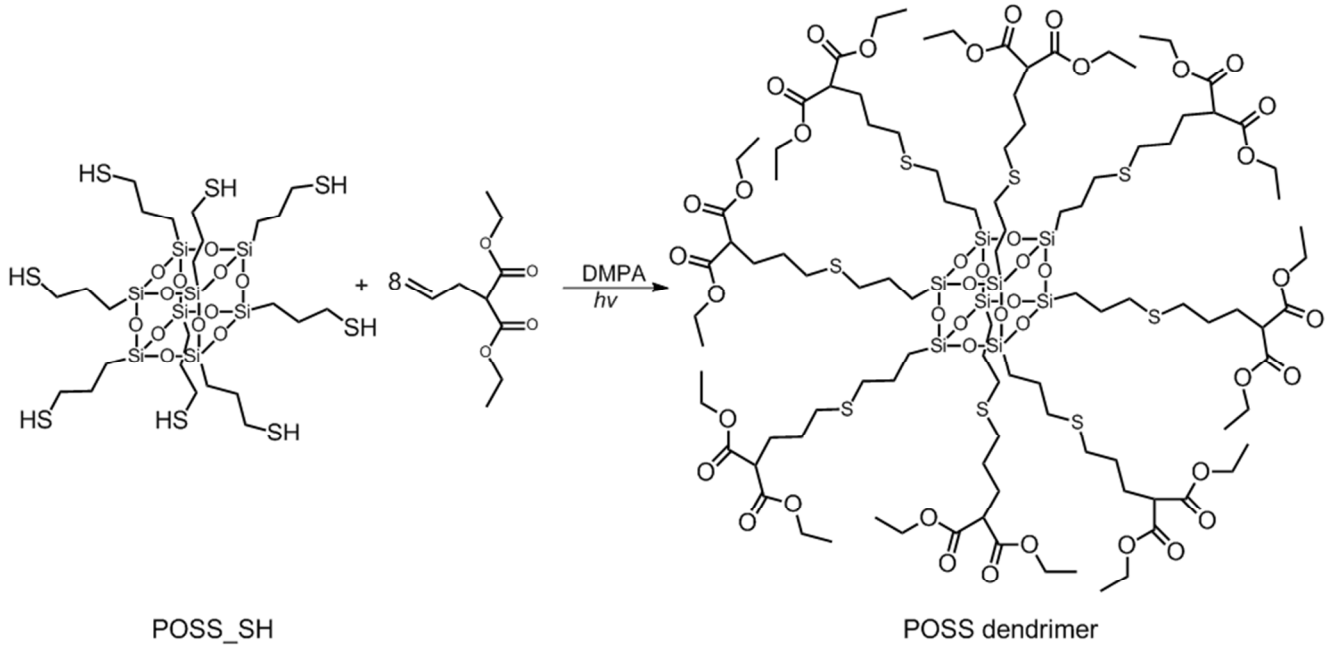

Scheme 1 Preparation of POSS_dendrimer.

Results and Discussion

Preparation of POSS_dendrimer

Thiol–ene reaction has been used to prepare some novel molecules and materials based on POSS. In most cases, the starting materials start from vinyl–substituted POSS, which has some limitations, especially when commercial thiol monomers are unavailable. This study selected octamercaptopropyl–substituted POSS (POSS_SH) as the starting material to react with diethyl allylmalonate to prepare diketone–functionalized POSS dendrimer (denoted as POSS_dendrimer) (Scheme 1).

The FT–IR spectra show that –SH (2552 cm^{-1}) disappeared in the spectrum of POSS_dendrimer after the reaction (Fig. S2). Subsequently, the characteristic absorption band of the carbonyl groups in the ketone appeared at 1730 cm^{-1}, and a strong band was associated with the asymmetric stretching of a siloxane framework near 1116 cm^{-1}. In the ^1H NMR spectrum of POSS_dendrimer, the signal of –SH (1.37 ppm) disappeared. These results strongly suggest that the reaction was complete. In addition, only one peak (−66.7 ppm) was observed in the ^{29}Si NMR spectrum of POSS_dendrimer, indicating that the POSS cage was kept intact during the reaction (Fig. S5). In addition, elemental analysis result suggested that the desired compound was formed. More importantly, the molecular ion peak of POSS–dendrimer (2847.77) unambiguously appeared in MALDI–FTMS spectrum (Fig. S7), corresponding to [M + dithranol + $H]^+$, which further indicated that this POSS_dendrimer was successfully synthesized *via* thiol–ene reaction.

Preparation of hybrid complexes based on POSS_dendrimer

A series of complexes (POSS_Ln) with different molar ratios of POSS and lanthanide ions (Eu^{3+} and Tb^{3+}) was prepared in THF

using POSS_dendrimer as a ligand. After THF removal, transparent solid films were obtained (Fig. S1a).

To demonstrate that the POSS_dendrimer had coordinated with the lanthanide ions, FT–IR was performed. Fig. 1a shows the FT–IR spectra of POSS complexes with Eu^{3+} and Tb^{3+}, respectively. A new band at approximately 1628 cm^{-1} appeared in the complexes, indicating the generation of C=C bond after coordination. The band at 1297 cm^{-1} became intense relative to the POSS_dendrimer, suggesting the increase of single C–O bond. Both bands suggested that the rare earth ions had successfully coordinated with the POSS_dendrimer. The increase in Eu^{3+} (Tb^{3+}) ion ratios resulted in the increase of intensity of the two bands. The generation of C=C bond and the enhancement of CO–O bond are attributed to the formation of keto–enol structure (Fig. 1b).[46–49] Given the coordination with rare earth ions, the keto–enol structure resulted in the formation of C=C bond, enhancement of CO–O bond, and weakness of C=O bond.

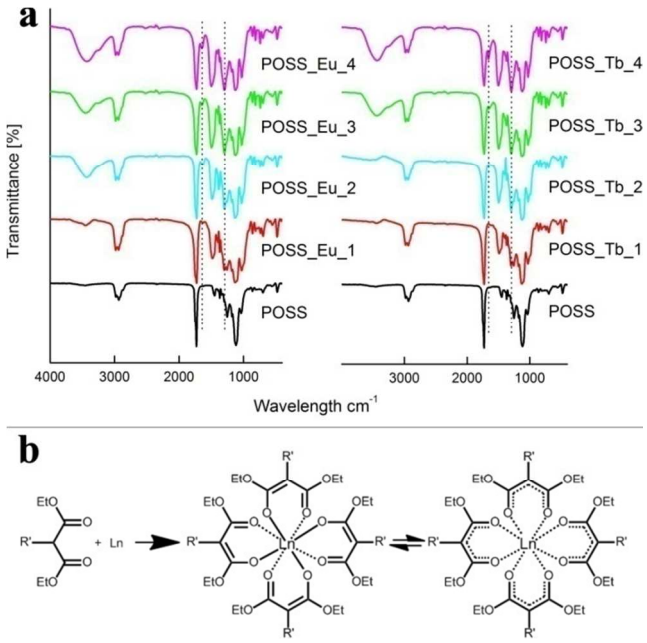

Fig. 1 (a) FT–IR spectra of POSS_Ln (Eu^{3+} and Tb^{3+}). (b) Schematic description of the keto–enol structure of the Ln–containing molecule.

XPS is an efficient technique to investigate the coordination process *via* the change of binding energy from inner acceptor to ambient ligands. To further confirm that coordination occurred between the POSS_dendrimer and the ions, the complexes were also subjected to XPS measurements. Considering the coordination similarity of these complexes, the XPS of POSS_Tb_3 was selected as an example in this study. The binding energy of Tb^{4d} shifted from 151.7 eV in terbium nitrate to higher binding energy at 153.3 eV in POSS_Tb_3 further confirmed the coordination of Ln^{3+} with POSS_Dendrimers occured (Fig. S8, Table S1).

Morphology of hybrid complexes

In many cases, the coordination bond between the central metal and the peripheral ligand is a driving force for their self–assembly behaviors in solid phases.[50] In this study, the coordination bond between the center rare earth ions (Eu^{3+} and Tb^{3+}) and the diketone groups is the driving force of the self–assembly of these hybrid luminescent materials. The morphology structure of these complexes based on POSS was investigated using PXRD, POM, SAXS, TEM, and DLS.

PXRD results showed that all the complexes were amorphous from 6° to 80° and exhibited no long–range order (Fig. S9) . All the samples exhibited broad diffraction peaks at 22.8°, which was typically observed in amorphous silica nanocomposites and associated with Si–O–Si linkage. To further investigate the crystallinity of these complexes, POM was also performed. POM images showed that some crystals existed in the matrix (Fig. S10). This finding suggested that certain crystalline regions existed in the complexes but were not reflected in the PXRD patterns because the crystalline peaks were concealed by POSS.

SAXS was used to investigate the self–assembly behaviors of the hybrid materials. The SAXS patterns showed that broad maxima existed in POSS_dendrimer and POSS_Ln with ratios of 1:2 and 1:3 and the peak position (q) was also observed to have shifted from 3.2 nm^{-1} to 2.6 nm^{-1}, which further confirmed that coordination occurred between POSS_dendrimer and rare earth ions (Fig. S11).

To further investigate the self–assembly behaviors of the hybrid complexes, TEM and DLS measurements were carried out. As shown in Fig 2, POSS_Eu_3 aggregated into small spherical particles with diameter range from 30 to 150 nm in TEM image; the average hydrodynamic diameter of this hybrid complex by DLS was about 100 nm and the size distribution was in accordance with the TEM result.

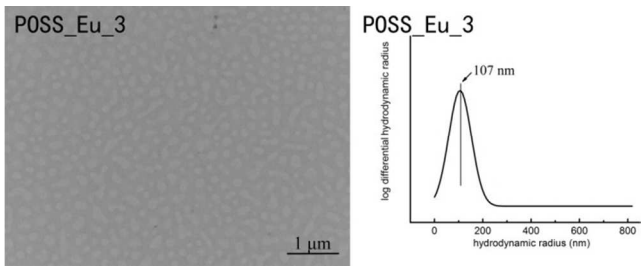

Fig. 2 TEM image and DLS figure of POSS_Eu_3.

Optical properties of these hybrid complexes

UV absorption of these complexes was carried out at room temperature. The UV spectra of POSS_Eu and POSS_Tb was displayed in Fig. S12. The absorption intensity was <1.5. Two absorption bands can be observed in Fig. S12. A strong absorption appearing at 249 nm corresponded to the π→π* electronic transition of diethyl malonate groups. The second band observed around 275 nm was attributed to n→π* electronic transition of keto carbonyl.[51–53] After coordination with rare earth ions, a portion of β–diketone structure in the POSS_Ln was converted into keto–enol structure (Fig. 1b). Thus, the absorption of keto carbonyl weakened. Meanwhile, the approximately 275 nm absorption band of the keto–enol structure group gradually increased with increasing ratios of rare earth ions. The UV spectra further demonstrated that rare earth ions were successfully coordinated with POSS_dendrimer.

The luminescent behaviors of POSS_Eu and POSS_Tb in solid state were studied at room temperature. The emission spectra of POSS_Eu and POSS_Tb show narrow–width characteristic emissions of Eu^{3+} and Tb^{3+}, respectively (Fig. 3). POSS_Eu

shows the narrow–width red emission bands located at 582, 595, 619 and 653 nm. These bands corresponded to the transitions between the different levels of Eu^{3+} and were attributed to $^5D_0 \rightarrow {}^7F_0$, $^5D_0 \rightarrow {}^7F_1$, $^5D_0 \rightarrow {}^7F_2$ and $^5D_0 \rightarrow {}^7F_3$ transitions of Eu^{3+} ions.[54–56] Bands in the 400 nm to 650 nm range can be clearly observed in the luminescence spectra of POSS_Tb, which are assigned to $^5D_4 \rightarrow {}^7F_6$, $^5D_4 \rightarrow {}^7F_5$, $^5D_4 \rightarrow {}^7F_4$ and $^5D_4 \rightarrow {}^7F_3$ transitions of Tb^{3+} in POSS_Tb at 491, 546, 586 and 625 nm, respectively.[57–59] Consequently, strong and characteristic luminescence were observed in the emission spectra. This finding indicates that effective intramolecular energy transfer occurred between the POSS_dendrimer and the cheated rare earth ions. The $^5D_0 \rightarrow {}^7F_2$ transition showed the strongest emission, suggesting that the chemical environment around Eu^{3+} ions was in low symmetry.[60] In addition, the asymmetric coordinative environment may have increased the probability for the electro–dipole transitions of Eu^{3+} ions. In the complexes with POSS system, the symmetry of Eu^{3+} ion coordination was rendered disorderly by the existence of NO_3^- and H_2O. The low symmetry around Eu^{3+} ion may increase the energy transfer probability and result in the enhancement of the fluorescence intensity of POSS_Eu complexes.[61]

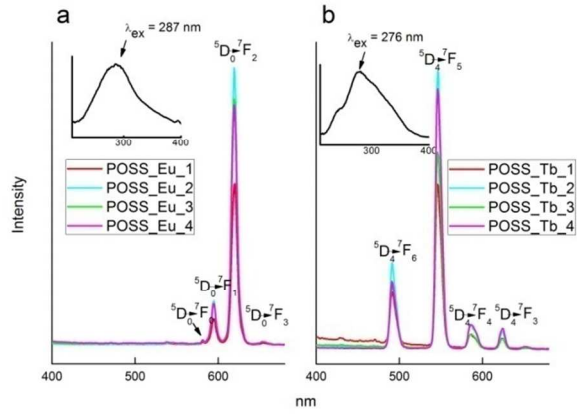

Fig. 3 Emission spectra of POSS_Ln (Eu^{3+} and Tb^{3+}) in solid state.

The fluorescence quantum yields (FQY) of the complexes were measured in THF solution and determined by the relative comparison procedure, using Quinine Sulfate in 0.05 M H_2SO_4 as the main standard. The corrected emission spectra were measured for the quinine sulfate standard (λ_{ex}=315 nm, A_r=0.05, quantum yield=0.508).[62] The general equation used in the determination of relative quantum yields is given in equation (1).[63]

$$Q_x=Q_r(A_r/A_x)(I_r/I_x)(n^2_x/n^2_r)(D_x/D_r) \quad (1)$$

Where Q is the quantum yield of the solution, A (λ) is the absorbance of the solution at the exciting wavelength λ, I (λ) is the relative intensity of the exciting light at wavelength λ, n is the average refractive index of the solution to the luminescence and D is the integrated area under the corrected emission spectrum. Subscript x and r refer to the unknown and reference solution, respectively.

The FQY of the POSS_Eu and POSS_Tb calculated in THF solution are listed in Table 2. Due to the different exciting energy of the POSS_Eu and POSS_Tb, there existed discrepancy in their QY. Meanwhile, their exciting energy was close, and the difference between them was slight.

Table 2 The FQY of POSS_Ln in THF solution.

Molar ratios	1:1	1:2	1:3	1:4
POSS_Eu	0.012	0.013	0.015	0.017
POSS_Tb	0.010	0.011	0.012	0.013

Hybrid luminescent PMMA nanocomposites from hybrid complexes (PMS_Ln)

The miscibility between hybrid complexes and MMA monomers was very good. After polymerization, the resulted hybrid PMMA nanocomposites were also transparent (Fig. 4). These hybrid PMMA nanocomposites with POSS exhibited excellent photoluminescence and monochromaticity when excited at 365 nm by a UV light (Fig. S1c). First, these hybrid PMMA materials were characterized by FTIR spectra (Fig. S14). FTIR results showed that there existed a strong abosorption band at 1730 cm^{-1}, corresponding to carbonyl stretching vibration, and aliphatic CH_2 bands at 3000–2845cm^{-1} in all spectra; the broad band from 1108 to 1148 cm^{-1}, corresponding to characteristic Si–O–Si vibrating modes, was found in the spectra of the hybrid nanocomposites and their intensities increase with increasing POSS content, indicating that POSS are indeed incorporated to PMMA matrix.

Fig. 4 Photographs of hybrid PMMA nanocomposites.

Wide angle X–ray diffraction was used to investigate the morphology and miscibility of hybrid nanocomposites (Fig. 5a). It was observed that pure PMMA and POSS_Ln_3 had a broad peak at 2θ ≈ 14°, 22°, respectively, indicating that they were amorphous. When POSS_Ln_3 was incorporated into PMMA matrix, a broader amorphous peak at 2θ ≈ 14° compared to pure PMMA appeared in the hybrid PMMA nanocomposites. It was a consequence of the overlapping two signals of POSS and pure PMMA for the low content of POSS_Ln. This meant that macrophase separation did not occur in this hybrid nanocomposites.[64,65] SAXS was also used to investigate the morphology structure of these hybrid PMMA nanocomposites. (Fig. 5b) It was found that the maxima of hybrid complexes disappeared after they were incorporated into PMMA matrix. This also suggested that hybrid complexes were well dispersed into PMMA matrix and large aggregation did not occur at least.

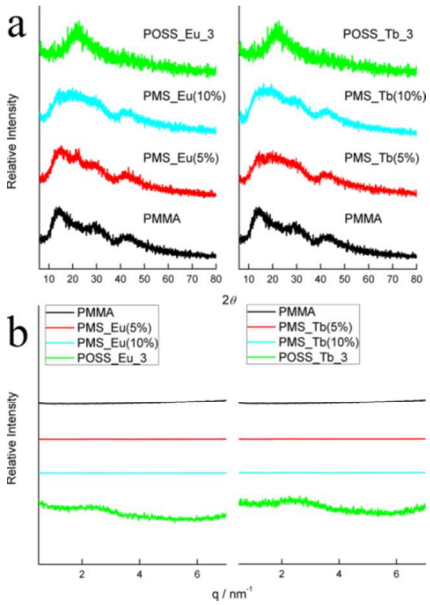

Fig. 5 (a) PXRD and (b) SAXS patterns of PMS_Ln (Eu^{3+} and Tb^{3+}).

To further confirm that the dispersion of POSS_Ln in PMMA matrix, TEM measurement was also conducted. PMS_Eu (5%) was selected as a representative sample considering their structural similarity. As shown in Fig. 6, it could be clearly seen that inorganic particles were well-dispersed in PMMA with sizes about 100 nm. The result demonstrated that POSS_Ln could be well distributed in PMMA without large-scale aggregation.

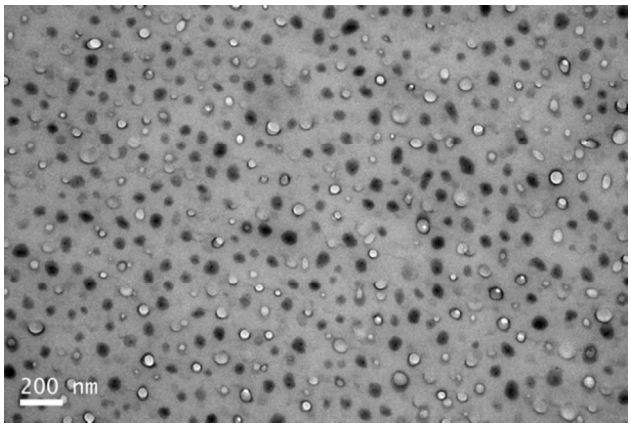

Fig. 6 TEM image of PMS_Eu (5%).

The PL spectra of hybrid nanocomposites with PMMA were also measured. The emission spectra of the nanocomposites has a profile similar to that of the hybrid complexes, indicative of the same kind of emission center except for a decrease in intensity due to their concentration in the PMMA matrix (Fig. S15). The FQY of PMS_Ln in solid state was also tested. The FQY of the PMS_Eu (5%) and PMS_Eu (10%) was 0.13%, 0.26% respectively; for PMS_Tb (5%) and PMS_Tb (10%), it was 0.16% and 0.31%, respectively. It was interesting that the fluorescence quantum yields (FQY) increased linearly with POSS_Ln loading, indicating that there existed energy transference from PMMA matrix to POSS_Ln. The coordination state of Ln^{3+} was actually unsaturated in POSS_Ln_3, and when POSS_Ln_3 was embedded into PMMA matrix, the carbonyl groups in PMMA could further coordinate with the unsaturated Ln^{3+}. When excited by the same light source, PMMA matrix with more POSS_Ln loading would exhibit higher FQY. Considering the low content of POSS_Ln (less than 10 %) in PMMA, almost all Ln^{3+} were coordinated with POSS ligands and/or PMMA. Therefore, the FQY was proportional to the content of POSS_Ln.

TGA was used to evaluate the thermal stability of hybrid PMMA nanocomposites (Fig. 7). Initial thermal decomposition temperature (T_d) is defined as the temperature at which the mass loss of 5 wt% occurs. First, the thermal stability of POSS_Ln was examined by TGA (Fig. S13). They exhibited similar thermal degradation behavior, i.e., two main degradation steps could be clearly observed in the TGA curves. The first weight loss before 280 °C could be attributed to the loss of physically absorbed and chemically conjugated water. T_d gradually decreased with the increase in molar ratio of Ln^{3+}. The second weight loss step could be ascribed to the decomposition of the organic groups, the coordinated $Eu(NO_3)_3$, and the degradation of the main framework of POSS cages. The weight loss rate decreased with increasing Ln ions; in addition, the residual mass increased with the increase of lanthanide. The thermal stabilities of PMS_Ln were also evaluated by TGA. Their thermal stabilities were indeed improved with incorporating POSS. The improvement in thermal stability was attributed to the nanoscale distribution of POSS_Ln in PMMA matrix, which inhibited the thermal decomposition of PMMA.[66] Moreover, the hybrid materials with high POSS_Ln displayed obviously increased char yield.

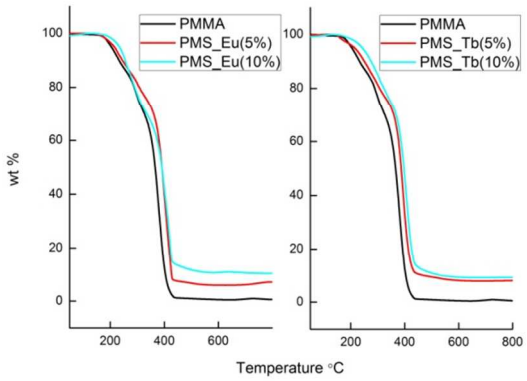

Fig. 7 Thermal gravimetric analysis of PMS_Ln (Eu^{3+} and Tb^{3+}) nanocomposites.

Conclusions

A new β–diketone–substituted dendrimer was successfully synthesized using POSS as cores *via* photochemical thiol–ene reaction. This POSS dendrimer was used as a ligand to coordinate with europium (III) ion and terbium (III) ion to obtain novel hybrid photoluminescent complexes. The hybrid complexes were embedded into PMMA matrix to form hybrid luminescent nanocomposites. The resultant PMMA nanocomposites based on POSS exhibited highly saturated color and good thermal stability.

The complexes and their nanocomposites with PMMA emitted narrow–width red or green luminescence by UV excitation. This finding suggests that the intramolecular energy transfer process

between the diketone group and the lanthanide ions occurred within these POSS–based hybrids. This study extends POSS applications in the luminescence field and represents an ideal approach for the improvement of thermal stability and mechanical processability of photoluminescent materials. These hybrid nanocomposites could be potentially used as 3D display materials and up–converters for photovoltaic applications, and this method may be extended to prepare other functional hybrid nanocomposites. Given the convenience of the route to multifunctional dendrimers using POSS, numerous dendrimer ligands based on POSS and their hybrid complexes or nanocomposites based on POSS are expected to be prepared in the future.

Acknowledgements

This research was supported by the National Natural Science Foundation of China (21274081).

Notes and references

Key Laboratory of Special Functional Aggregated Materials, Ministry of Education, School of Chemistry and Chemical Engineering, Shandong University, Jinan 250100, P. R. China Tel: +86 531 88364691; E–mail: liuhongzhi@sdu.edu.cn

† Electronic Supplementary Information (ESI) available: FT–IR spectra, NMR spectra and MALDI–FTMS spectrum of POSS_dendrimer, XPS results, PXRD figures, UV spectra, TGA curves, Photo graphs and POM images of POSS_Ln, FT–IR spectroscopy, and PL spectra of PMS_Ln. See DOI: 10.1039/b000000x/

1 K. Binnemans, *Chem. Rev.*, 2009, **109**, 4283–4374.
2 Y. Huang, F. Jiang and M. Hong, *Coord. Chem. Rev.*, 2009, **253**, 2814–2834.
3 L. Carlos, R. Ferreira, V. Bermudez, B. Julian–Lopez and P. Escribano, *Chem. Soc. Rev.*, 2011, **40**, 536–549.
4 Z. Zhang, G. Chen and J. Liu, *RSC Adv.*, 2014, **4**, 7991-7997
5 S. Aime, M. Botta, M. Fasano and E. Terreno, *Chem. Soc. Rev.*, 1998, **27**, 19–29.
6 R. Kumar, M. Nyk, T. Ohulchanskyy, C. Flask and P. Prasad, *Adv. Funct. Mater.*, 2009, **19**, 853–859.
7 K. Kuriki, Y. Koike and Y. Okamoto, *Chem. Rev.*, 2002, **102**, 2347–2356.
8 R. Crooks, M. Zhao, L. Sun, V. Chechik and L. Yeung, *Acc. Chem. Res*., 2001, **34**, 181–190.
9 S. Sevenson and D. Tomalia, *Adv. Drug Deliv. Rev*., 2005, **57**, 2106–2129.
10 C. Goltner, B. Smarsly, B. Berton and M. Antonietti, *Chem. Mater*., 2001, **13**, 1674–1624.
11 C. Pitois, A. Hult and M. Lindgren, *J. Lumin.*, 2005, **111**, 265–283.
12 M. Alcala, C. Shade, H. Uh, S. Kwan, M. Bischof, Z. Thompson, K. Gogick, A. Meier, T. Strein and D. Bartlett, *Biomaterials*, 2011, **32**, 9343–9352.
13 M. Kawa and J. Frechet, *Thin Solid Films*, 1998, **331**, 259–263.
14 V. Vicinelli, P. Ceroni, M. Maestri, V. Balzani, M. Gorka and F. Vogtle, *J. Am. Chem. Soc*., 2002, **124**, 6461–6168.
15 B. Branchi, P. Ceroni, V. Balzani, F. Klarner and F. Vogtle, *Chem. Eur. J*., 2010, **16**, 6048–6055.
16 D. Cordes, P. Lickiss and F. Rataboul, *Chem. Rev.*, 2010, **110**, 2081–2173.
17 H. Liu, S. Kondo, N. Takeda and M. Unno, *J. Am. Chem. Soc*., 2008, **130**, 10074–10075.
18 S. Kuo and F. Chang, *Prog. Polym. Sci.*, 2011, **36**, 1649–1696.
19 A. Luo, X. Jiang, H. Lin and J. Yin, *J. Mater. Chem.*, 2011, **21**, 12753–12760.
20 J. Furgal, J. Jung, T. Goodson and R. Laine, *J. Am. Chem. Soc.*, 2013, **135**, 12259–12269.
21 R. Laine, S. Sulaiman, C. Brick, M. Roll, R. Tamaki, M. Asuncion, M. Neurock, J. Filhol, C. Lee and J. Zhang, *J. Am. Chem. Soc.*, 2010, **132**, 3708–3722.
22 C. He, Y. Xiao, J. Huang, T. Lin, K. Mya and X. Zhang, *J. Am. Chem. Soc.*, 2004, **126**, 7792–7793.
23 M. Lo, C. Zhen, M. Lauters, G. Jabbour and A. Sellinger, *J. Am. Chem. Soc*,. 2007, **129**, 5808–5809.
24 C. Lu, S. Kuo, C. Huang and F. Chang, *J. Phys. Chem. C*, 2009, **113**, 3517–3524.
25 Y. Wang, A. Vaneski, H. Yang, S. Gupta, F. Hetsch, S. Kershaw, W. Teoh, H. Li and A. Rogach, *J. Phys. Chem. C*, 2013, **117**, 1857–1862.
26 X. Zhao, J. Du, Y. Wu, H. Liu and X. Hao, *J. Mater. Chem. A*, 2013, **1**, 11748–11753.
27 S. Spoljaric and R. Shanks, *J. Appl. Polym. Sci.*, 2012, **126**, E440–E454.
28 H. Batista, A. de Andrade, R. Longo, A. Simas, G. de Sa, N. Ito and L. Thompson, *Inorg. Chem.*, 1998, **37**, 3542–3547.
29 R. Zhang, K. Yang, A. Yu and X. Zhao, *Thin Solid Films*., 2000, **363**, 275–278.
30 C. Molina, K. Dahmouche, Y. Messaddeq, S. Ribeiro, M. Silva, V. Bermudez and L. Carlos, *J. Lumin*., 2003, **104**, 93–101.
31 L. Carlos, R. Ferreira, V. Bermudez and S. Ribeiro, *Adv. Mater*., 2009, *21*, 509–534.
32 J. Feng and H. Zhang, *Chem. Soc. Rev*., 2013, **42**, 387–410.
33 X. Chen, P. Zhang, T. Wang, H. Li, *Chem. Eur. J*., 2014, **20**, 2551 – 2556.
34 J. Boyer, N. Johnson and F. van Veggel, *Chem. Mater*., 2009, **21**, 2010–2012.
35 H. Althues, R. Palkovits, A. Rumplecker, P. Simon, W. Sigle, M. Bredol, U. Kynast and S. Kaskel, *Chem. Mater*., 2006, **18**, 1068–1072.
36 H. Zhang, C. Wang, M. Li, J. Zhang, G. Lu and B. Yang, *Adv. Mater*., 2005, **17**, 853–857.
37 R. Gangopadhyay and A. De, *Chem. Mater*., 2000, **12**, 608–622.
38 P. Gomez–Romero, *Adv. Mater*., 2001, **13**, 163–174.
39 C. Guan, C. Lu, Y. Cheng, S. Song and B. Yang, *J. Mater. Chem*., 2009, **19**, 617–621.
40 D. Cristaldi, S. Millesi, P. Mineo and A. Gulino, *J. Phys. Chem. C*., 2013, **117**, 16213–16220.
41 A. Gulino, F. Lupo, G. Condorelli, A. Motta and I. Fragala, *J. Mater. Chem*., 2009, **19**, 3507–3511.
42 J. Fu, L. Shi, Y. Chen, S. Yuan, J. Wu, X. Liang and Q. Zhong, *J. Appl. Polym. Sci*., 2008, **109**, 340–349.
43 K. Bouhadir, J. Zhou and P. Shevlin, *Synth. Commun*., 2005, **35**, 1003–1010.
44 J. Mazzolini, O. Boyron, V. Monteil, D. Gigmes, D. Bertin, F. D'Agosto and C. Boisson, *Macromolecules*, 2011, **44**, 3381–3387.
45 N. Cramer, T. Davies, A. O'Brien and C. Bowman, *Macromolecules*., 2003, **36**, 4631–4636.
46 H. Kim, Y. Kim and J. Chang, *J. Polym. Sci., Part A: Polym. Chem*., 2012, **50**, 4990–4994.
47 B. Hall and J. Brodbelt, *J. Am. Soc. Mass. Spectrom*., 1999, **10**, 402–413.
48 R. Claramunt, C. Lopez, M. Maria, D. Sanz and J. Elguero, *Prog. Nucl. Magn. Reson. Spectrosc*., 2006, **49**, 169–206.
49 J. Kai, D. Parra and H. Brito, *J. Mater. Chem*., 2008, **18**, 4549–4554.
50 X. Li, W. Xu, H. Jia, X. Wang, B. Zhao, B. Li and Y. Ozaki, *J. Colloid Interface Sci*., 2004, **274**, 9–15.
51 Z. Chen, Y. Wu, F. Huang, D. Gu and F. Gan, *Spectrochim. Acta. Part A*., 2007, **66**, 1024–1029.
52 A. El–Sonbati, M. Diab, A. Belal and S. Morgan, *Spectrochim. Acta. Part A*., 2012, **99**, 353–360.
53 Q. Lai, H. Lu, D. Wang, H. Wang, S. Feng and J. Zhang, *Macromol. Chem. Phys*., 2011, **212**, 1435–1442.
54 V. Taxak, Sheetal, Dayawati and S. Khatkar, *Current Applied Physics*., 2013, **13**, 594–598.
55 Q. Zhao, N. Guo, Y. Jia, W. Lv, B. Shao, M. Jiao and H. You, *J. Colloid Interface Sci*., 2013, **394**, 216–222.

56 H. Hara, S. Takeshita, T. Isobe, T. Sawayama and S. Niikura, *Mater. Sci. Eng. B*., 2013, **178**, 311–315.
57 E. Kusrini, M. Saleh, R. Adnan, Y. Yulizar and M. Mamat, *Spectrochim. Acta, Part A.,* 2012, **98**, 322–328.
58 P. Nagpure and S. Omanwar, *J. Rare Earth*., 2012, **30**, 856–859.
59 A. Podhorodecki, N. Gaponenko, M. Banski, M. Rudenko, L. Khoroshko, A. Sieradzki and J. Misiewicz, *Opt. Mater*., 2012, **34**, 1570–1574.
60 Y. Li, B. Yan and H. Yang, *J. Phys. Chem. C*., 2008, **112**, 3959–3968.
61 R. Velapoldi and H. Tonnesen, *J. Fluoresc.*, 2004, **14**, 465-472.
62 J. Demas and G. Crosby, *J. Phys. Chem.*, 1971, **75**, 991–1024.
63 D. Liu, Z. Wang, H. Yu and J. You, *Eur. Polym. J*., 2009, **45**, 2260–2268.
64 E. Kopesky, T. Haddad, G. McKinley and R. Cohen, *Polymer*, 2005, **46**, 4743–4752.
65 M. Saladino, A. Zanotto, D. Martino, A. Spinella, G. Nasillo and E. Caponetti, *Langmuir*, 2010, **26**, 13442–13449.
66 Y. Wu, L. Li, S. Feng and H. Liu, *Polym. Bull*., 2013, **70**, 3261–3277.